Cell confinement controls centrosome positioning and lumen initiation during epithelial morphogenesis

Alejo E. Rodríguez-Fraticelli,[1] Muriel Auzan,[2] Miguel A. Alonso,[1] Michel Bornens,[3] and Fernando Martín-Belmonte[1]

[1]Centro de Biología Molecular Severo Ochoa, Consejo Superior de Investigaciones Científicas-Universidad Autónoma de Madrid, 28049 Madrid, Spain
[2]CYTOO SA, Commissariat à l'Energie Atomique et aux Energies Alternatives Grenoble, 38054 Grenoble, Cedex 09, France
[3]Unité Mixte de Recherche 144, Centre National de la Recherche Scientifique, Institut Curie, 75006 Paris, Cedex 05, France

Epithelial organ morphogenesis involves sequential acquisition of apicobasal polarity by epithelial cells and development of a functional lumen. In vivo, cells perceive signals from components of the extracellular matrix (ECM), such as laminin and collagens, as well as sense physical conditions, such as matrix stiffness and cell confinement. Alteration of the mechanical properties of the ECM has been shown to promote cell migration and invasion in cancer cells, but the effects on epithelial morphogenesis have not been characterized. We analyzed the effects of cell confinement on lumen morphogenesis using a novel, micropatterned, three-dimensional (3D) Madin-Darby canine kidney cell culture method. We show that cell confinement, by controlling cell spreading, limits peripheral actin contractility and promotes centrosome positioning and lumen initiation after the first cell division. In addition, peripheral actin contractility is mediated by master kinase Par-4/LKB1 via the RhoA–Rho kinase–myosin II pathway, and inhibition of this pathway restores lumen initiation in minimally confined cells. We conclude that cell confinement controls nuclear–centrosomal orientation and lumen initiation during 3D epithelial morphogenesis.

Introduction

Epithelial organs are essentially formed by a monolayer of epithelial cells surrounding a central lumen. Lumen formation is a sequential process during which individually polarized cells differentiate and acquire collective apicobasal polarity. The ECM provides the initial cue that orients the apicobasal polarity axis, which is regulated by the activities of β1 integrin, Rac1 GTPase, and laminin, a component of the basal epithelial ECM (O'Brien et al., 2001; Yu et al., 2005). Once oriented, the apicobasal axis directs apical vesicle trafficking toward cell–cell junctions to initiate the process of lumen formation (Bryant and Mostov, 2008). In addition, the physiological extracellular environment of epithelial cells, comprising a wide array of physical stimuli, including tissue stiffness, water tension, and cell confinement, is perceived by cells through a process termed mechanotransduction, which is essential for cell shape, development, and tissue homeostasis (DuFort et al., 2011). Recent advances have established the importance of mechanotransduction in the regulation of tumor progression and cancer cell migration (Butcher et al., 2009). However, analysis of individual properties of the extracellular physical environment has remained a challenge for many years. Micropatterned adhesive surfaces have proved a key tool for the analysis of the interactions between ECM and cell morphogenesis in a wide variety of models (Théry, 2010). For example, cell confinement on micropatterns has been shown to regulate the assembly and orientation of the primary cilium in single epithelial cells (Pitaval et al., 2010). Despite these advances, however, no studies have yet addressed the role of cell confinement in the acquisition of 3D cell polarity and lumen formation, which are essential physiological processes in epithelial organs.

To analyze the effect of cell confinement on lumen formation, we devised a method to control the adhesive microenvironment (i.e., the components and size of the adhesive matrix) using micropatterned surfaces coated with either collagen or laminin to induce 3D lumen formation from single MDCK cells. Using this

Correspondence to Fernando Martín-Belmonte: fmartin@cbm.uam.es

Abbreviations used in this paper: aPKC, atypical PKC; BB, blebbistatin; dox, doxycycline; GEF, guanine nucleotide exchange factor; KD, knockdown; ROCK, Rho kinase; PS, pseudosubstrate; shRNA, small hairpin RNA.

The Rockefeller University Press $30.00
J. Cell Biol. Vol. 198 No. 6 1011–1023
www.jcb.org/cgi/doi/10.1083/jcb.201203075

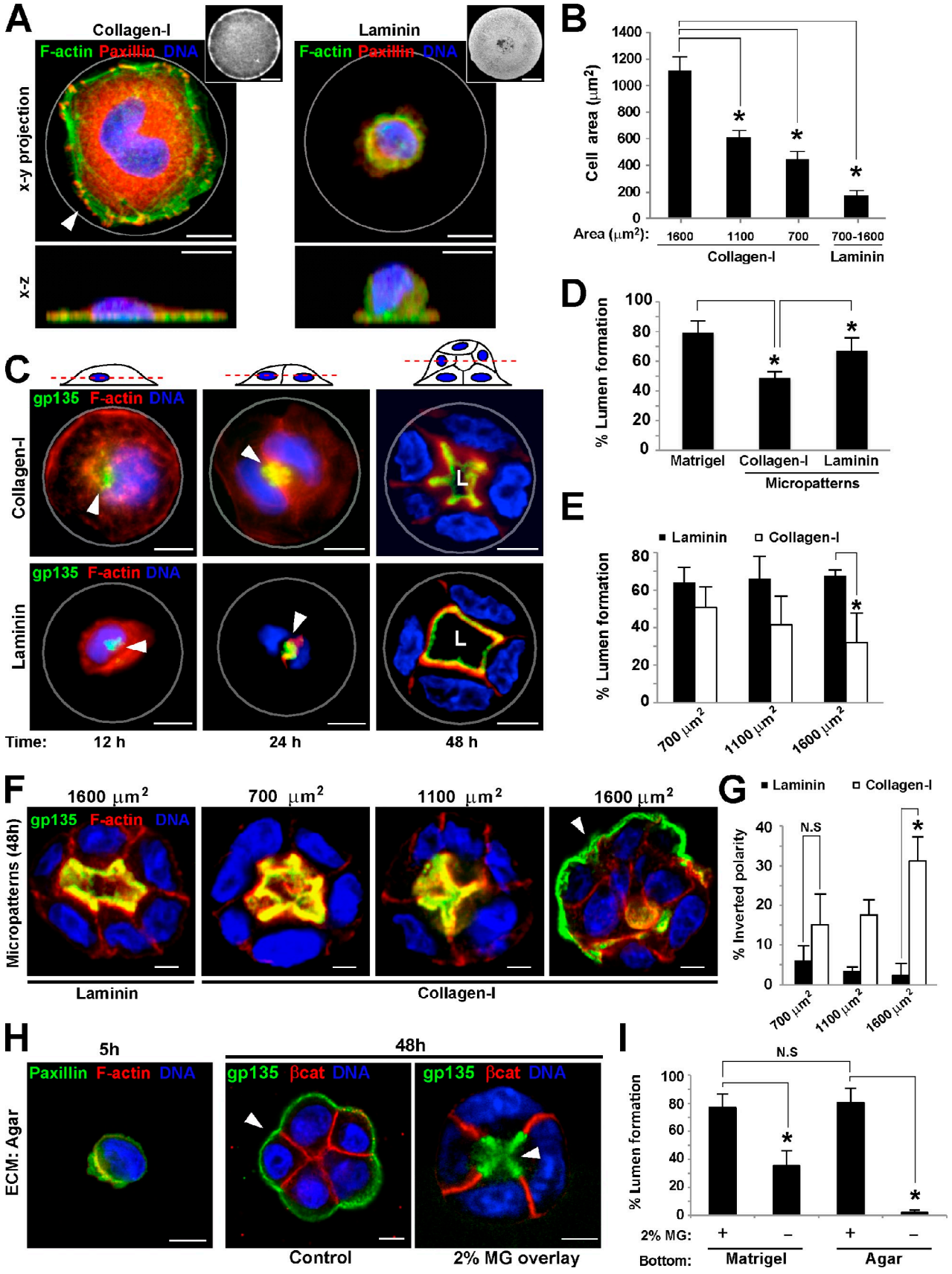

Figure 1. **Cell confinement in micropatterned surfaces regulates lumen formation.** (A) MDCK cells spreading on collagen I or laminin micropatterns. MDCK cells were seeded on 1,100-μm²-diam disk-shaped micropatterns using CYTOOchips. Cells were fixed 5 h after seeding. Cells were stained to detect F-actin, paxillin, and DNA and analyzed with confocal microscopy (maximum z projection). Micropattern collagen I or laminin staining is shown in the

method, we show that cell confinement regulates lumen initiation by modulating actin-mediated contractility from early cell aggregates to fully polarized epithelial tissues.

Results

Cell confinement regulates apicobasal polarity orientation and lumen formation

Confluent MDCK cells are typically grown in a 2D support and develop into a polarized columnar epithelium, in which the apical membrane forms by default at the only membrane domain in contact with the free medium. Upon reaching confluence, addition of ECM components generates a 3D cue that induces the formation of multicellular tubules in which cells develop a central lumen, separated from the surrounding medium (Ojakian et al., 1997). Lumen formation and apical membrane positioning have been traditionally studied in cells cultured at high confluence or using soft matrices, which prevent cell spreading and induce conditions similar to high cell confinement. As such, the contribution of cell confinement and cell spreading during the acquisition of epithelial cell polarity and lumen formation remains unknown. To address this issue, we first analyzed the effect of cell confinement on cell spreading using single epithelial cells seeded in disk-shaped micropatterns coated with different ECM substrates. Cells plated on collagen spread flat to cover the entire surface of the micropattern and formed extensive focal adhesions (visualized by paxillin staining), whereas those plated on laminin were taller and failed to spread or form focal adhesions, regardless of micropattern size (Fig. 1 A). Furthermore, in contrast to collagen-plated cells, in which cell spreading and focal adhesion formation depended on the surface area of the micropattern, cell spreading of laminin-plated cells was dramatically reduced regardless of micropattern size (Fig. 1 B and Fig. S1, A and B).

To investigate the effect of cell spreading on epithelial lumen formation, we seeded MDCK cells on disk-shaped micropatterns with Matrigel-supplemented medium to form 3D cysts and stained for the apical marker gp135/podocalyxin and F-actin to determine apical membrane localization. Interestingly, cells on collagen-coated micropatterns developed normal cysts with single central lumens (Fig. 1 C, top; Fig. S1, E and F; and Video 1), although less efficiently than cells cultured on laminin-coated micropatterns, in which lumen formation efficiency resembled that observed in normal 3D culture conditions (Fig. 1, C [bottom] and D). The observed improvement in normal lumen yield on laminin-coated micropatterns is consistent with previous studies, which found that laminin is required to orient apical–basal polarity in collagen gels (O'Brien et al., 2001; Yu et al., 2005). More importantly, our results suggested that physical confinement promotes 3D epithelial polarization and central lumen formation.

To test this hypothesis, we analyzed the role of cell confinement in lumen formation by plating MDCK cells on collagen I–coated micropatterns of different sizes. When cells were cultured on large micropatterns (low confinement conditions; 1,600 μm^2), we observed a significant increase in inverted polarity phenotypes and a reduction in lumen formation (Fig. 1, E–G). In contrast, culture of cells on smaller surfaces (high confinement conditions; 700 μm^2) resulted in a significant increase in the efficiency of lumen formation (Fig. 1, E–G). Cysts grown on laminin-coated micropatterns exhibited high lumen formation efficiencies independent of micropattern size (Fig. 1 E). To rule out a collagen I–specific effect, we cultured MDCK cells on micropatterns lacking any ECM substrate and observed similar results to those seen for collagen I–treated cells, although cell spreading was diminished, and the efficiency of lumen formation was slightly increased (Fig. S1, E and F). Collectively, these results indicate that high cell confinement promotes lumen formation under conditions that induce cell spreading, such as collagen I, and suggests that laminin signaling, which plays a key role in the orientation of cell polarity, also contributes to epithelial polarity by inhibiting cell spreading. Alternatively, laminin could diffuse into the basal side of the cell aggregates more easily in small micropatterns to promote cell polarization. We found, however, that laminin was exclusively deposited on the dorsal side of the cell aggregates, independent of cell confinement (Fig. S1 G). Thus, laminin diffusion does not alter lumen initiation in different cell confinement conditions.

To confirm the effect of cell confinement on lumen formation, we developed a novel method of cyst culture on agar, which prevents cell spreading (Discher et al., 2005). MDCK cells plated on agar mimicked the behavior of laminin-plated cells 5 h after

small top right insets. Arrowhead shows stress fibers. (B) Quantification of MDCK cell spreading in micropatterns of varying surface area (1,600, 1,100, and 700 μm^2) coated with collagen I or laminin. $n \geq 10$ cells/experiment. (C) Lumen formation in micropatterned MDCK cysts. MDCK cells were seeded on disk-shaped micropatterns (1,100 μm^2) coated with collagen I or laminin and grown to form cysts. Cysts were fixed at 12, 24, and 48 h. Samples were stained for gp135, F-actin, and DNA and analyzed with confocal microscopy. A scheme indicates the z plane shown in each image. Arrowheads indicate position of the apical membranes. L indicates the lumen. (D) Quantification of lumen formation in micropatterned MDCK cysts. MDCK cells were cultured to form cysts on collagen I– or laminin-coated micropatterns or cultured to form cysts on Matrigel (control). Cysts were fixed at 72 h, and normal lumen formation was quantified. $n \geq 30$ cysts/experiment. (E) Quantification of lumen formation efficiency in MDCK cysts formed on collagen- or laminin-coated micropatterns of different sizes (1,600, 1,100, and 700 μm^2). Cysts were fixed at 60 h, and normal lumen formation efficiency was quantified. $n \geq 30$ cysts/experiment. (F) Lumen formation in MDCK cysts using micropatterns of different sizes. MDCK cells were seeded on collagen I– or laminin-coated micropatterns of different sizes (1,600, 1,100, and 700 μm^2) and grown to form cysts. Cysts were fixed after 60 h and stained to detect gp135, F-actin, and DNA. Cysts were analyzed by confocal microscopy (central z slice is shown). Arrowhead indicates inverted apical polarity. (G) Quantification of cysts with inverted polarity in micropatterns of different sizes. MDCK cells were cultured to form micropatterned cysts, and the percentage of inverted apical polarity phenotypes was quantified. $n \geq 30$ cysts/experiment. (H) Cell spreading and lumen formation in MDCK cysts on soft agar. MDCK cells were seeded on agar-coated coverslips, fixed after 5 h, and stained to detect paxillin, F-actin, and DNA. Otherwise, MDCK cells were overlaid with 2% Matrigel-supplemented complete medium or nonsupplemented control medium. Cysts were cultured for 72 h and then fixed and stained to detect gp135, β-catenin, and DNA. Cysts were analyzed by confocal microscopy (central z slice is shown). Arrowheads indicate apical membrane localization. (I) Quantification of lumen formation on Matrigel or on soft agar, with or without 2% Matrigel (MG) overlay. $n \geq 50$ cysts/experiment. Values are means ± SD from three independent experiments. *, $P < 0.005$. Gray circles indicate micropattern shape. Bars, 5 μm.

System	Support	Medium	Bottom ECM	Cell spreading	Lumen formation	Scheme
Matrigel (3D-MDCK)	Matrigel	Matrigel	Matrigel	No	High	
2D-monolayers	Glass	MEM	None	Cell confluence-dependent	No lumens	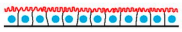
3D-monolayers	Glass	Matrigel-supplemented MEM	Laminin Collagen-I	Low High	High Very low	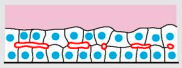
2D-micropatterns	Micropatterns	MEM	Laminin Collagen-I	Low Cell confinement-dependent	No	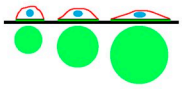
3D-micropatterns	Micropatterns	Matrigel-supplemented MEM	Laminin Collagen-I	Low Cell confinement-dependent	High Cell confinement-dependent	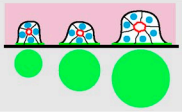
Agar	Agar gel	Matrigel-supplemented MEM	Agar	No	Yes	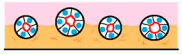

Apical membranes · Nuclei · Micropatterns · Agar · Matrigel · Matrigel-supplemented medium

Figure 2. **Culture systems to analyze lumen formation using MDCK cells.** Description of MDCK cell culture systems. The table summarizes cell support, bottom ECM coating, and culture medium and provides information on cell spreading behavior and lumen formation in each condition. The right column shows a scheme of an x-z section of each culture system, indicating position of cells and apical membranes in different ECM supports. Additionally, in micropattern culture systems, an x-y view of micropatterns and their different sizes is also shown.

seeding (Fig. 1 H, left). When cells were grown for 72 h on agar in 2% Matrigel-supplemented medium, we observed significant cyst formation, with correct positioning of the apical membrane and comparable efficiency to MDCK cells plated in normal 3D cyst culture conditions (Fig. 1 H). Lumen formation on agar was highly dependent on Matrigel supplementation of the culture medium (Fig. 1 I). Collectively, these findings indicate that cell confinement suffices to promote lumen formation regardless of the substrate to which the cells are attached.

Of the many different culture techniques used, the 3D micropatterned MDCK method on collagen was the only one that afforded precise control of cell spreading and cell confinement (Fig. 2). Thus, to characterize the mechanism that regulates lumen formation, we performed all subsequent analyses using collagen I–coated micropatterns of different sizes.

Peripheral actin contractility induced by cell spreading impairs nuclear-centrosomal positioning and lumen initiation

The actin cytoskeleton is a mechanical biosensor that detects modifications in the surrounding environment and modifies cell behavior and shape to control cellular processes, such as migration and polarity (Li and Gundersen, 2008). To analyze in detail the effect of cell confinement on lumen formation and the actin cytoskeleton, we tracked actin dynamics by live-cell microscopy using a fluorescent F-actin probe (GFP-Life-actin) in MDCK cells on collagen I–coated micropatterns of different sizes. At the time of seeding, F-actin was concentrated in stress fibers and other peripheral structures, such as lamellipodia (Fig. 3 A, left; and Videos 2 and 3). After the first cell division, F-actin was progressively enriched at cell–cell contacts. Interestingly, actin localization was polarized almost exclusively to cell–cell contacts in high cell confinement conditions (700 μm^2). The lumen was visible after 10 h and fully opened at 24 h (Fig. 3 A, top, arrowheads). In contrast, cells in low confinement conditions exhibited more peripheral actin structures after the first cell division. Moreover, lumen formation in low confinement was substantially delayed, and cell morphology in the aggregates differed significantly from cell to cell (Fig. 3, A [bottom, arrows] and B [quantification]). Quantitative analysis revealed that lumens formed faster and more efficiently in high versus low confinement conditions (Fig. 3 C and Fig. S2 A). However, the final number of cells was similar in high and low confinement, indicating that cell proliferation was not significantly affected (Fig. 3 A, right). Collectively, these results suggest that peripheral actin contractility is increased in cells in low confinement conditions, which delays early apicobasal cell polarization and lumen initiation after the first cell division. Moreover, these findings indicate that regulation of apical membrane positioning is defined immediately after the first cell division. In subsequent experiments, we thus assessed the contribution of cell confinement to cell polarity and lumen initiation using two-cell early aggregates (24 h) grown on collagen I–coated micropatterns of different sizes.

In animal cells, the centrosome, the main microtubule-organizing center, is a key organelle for cell polarity (Bornens, 2012). In division, the centrosomes organize the mitotic spindle, which should be properly oriented for normal lumen formation (Jaffe et al., 2008). One possible explanation to our findings is that the orientation of cell division might change in different confinement conditions and thereby differentially affects the formation of the lumen. However, we observed that the orientation of the first cell

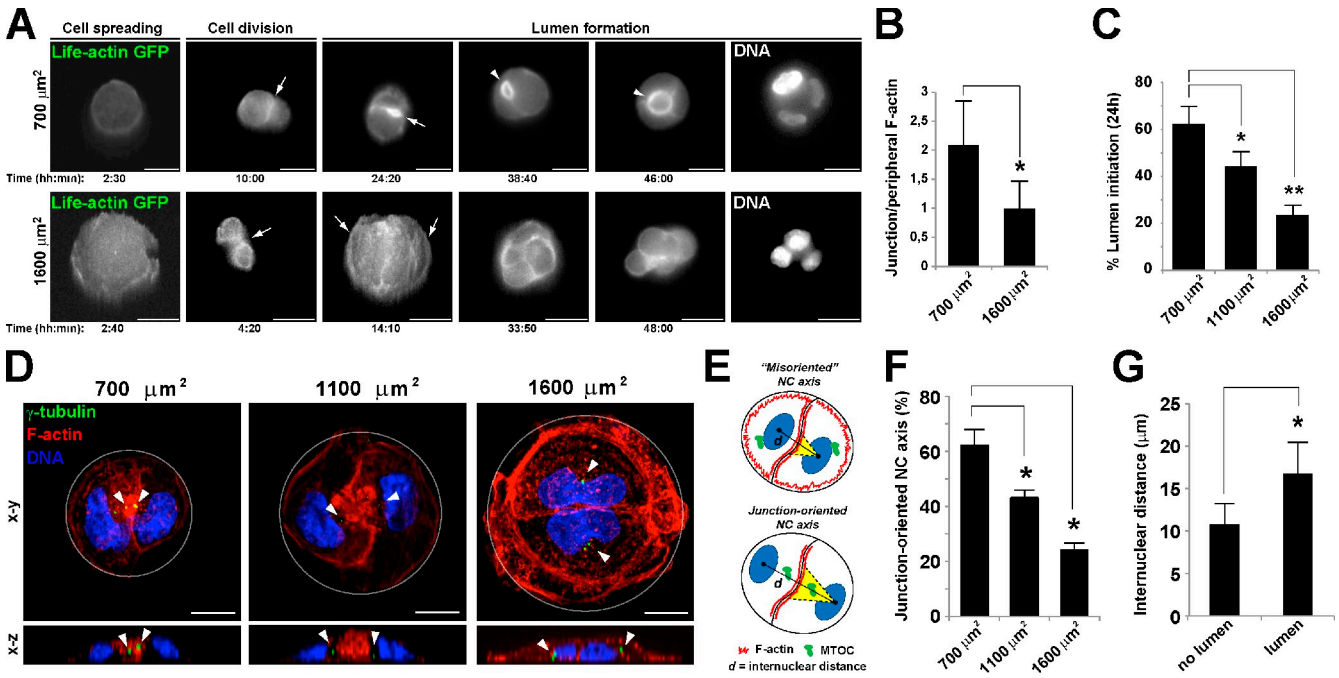

Figure 3. **Cell confinement regulates nuclear–centrosomal axis orientation after the first cell division.** (A) Life-actin-GFP localization during cyst formation in different confinement conditions. Life-actin-GFP MDCK cells were seeded on collagen I micropatterns of different sizes (700 and 1,600 µm^2) to grow cysts and analyzed by video microscopy for 48 h (one frame = 10 min). After 48 h, DNA was stained with cell-permeable Hoechst to show nuclei. Cysts contained an aggregate of approximately four cells, of which three nuclei are visible in the same plane. Still images were selected at different time points, and in some cases, intensity was enhanced to facilitate visualization of cell structures. Arrows indicate accumulation of actin at the cell–cell junctions or peripheral actin fibers. Arrowheads indicate lumen. Bars, 20 µm. (B) Quantification of polarization of actin during micropatterned cyst formation in collagen. Life-actin-GFP signal was analyzed after first cell division using live-cell imaging. The ratio between Life-actin fluorescent signal at junctions and periphery was quantified ($n = 6$; *, $P < 0.05$). (C) Quantification of lumen initiation in collagen I micropatterned cysts at 24 h. $n \geq 50$ cysts/experiment; *, $P < 0.005$; **, $P < 0.001$. (D) Centrosome orientation in micropatterned MDCK cells. MDCK cells were seeded to grow cysts on collagen I–coated micropatterns of different sizes and fixed after 20 h. Cells were stained for F-actin, γ-tubulin, and nuclei. Cells were analyzed by confocal microscopy (z-stack projections and x-z cross sections are shown). Gray circles indicate micropattern shape. Arrowheads indicate position of the centrosome. Bars, 10 µm. (E) Scheme of procedures for quantification of centrosome and nuclear positioning in cell doublets. Distances between nuclei are quantified (*d*). The orientation of the nucleus–centrosome (NC) axis is considered incorrect (misoriented) when the centrosome is facing the periphery and correct (junction oriented) when the centrosome is within the 90° quadrant formed between the nucleus and the cell–cell junctions. MTOC, microtubule-organizing center. (F) Quantification of centrosome positioning in different confinement conditions. $n \geq 30$ cysts/experiment; *, $P < 0.005$. (G) Quantification of internuclear distance. $n \geq 30$ cysts/experiment; *, $P < 0.005$. Values are means ± SD from three independent experiments.

division is not significantly changed using micropatterns of different sizes (Fig. S2, B–D). On the other hand, the components of the vesicular trafficking pathway that regulates lumen formation are repositioned together with the centrosome, which orients toward the apical pole as epithelial cells differentiate (Datta et al., 2011). It remains unclear though whether centrosome positioning is essential for lumen formation (Rodríguez-Fraticelli et al., 2011). To determine the effect of cell confinement on centrosome localization, we analyzed the position of centrosomes in MDCK cells cultured on collagen-coated micropatterns of different sizes. After cell division in high confinement conditions, most centrosomes were oriented toward the lumen initiation site at the center of the micropattern, whereas the centrosomes of cells in low confinement conditions were predominantly oriented toward the periphery (Fig. 3, D–F; and Fig. S2, E and F). In addition, Golgi apparatus was polarized toward the junctions in high confinement, thus essentially mimicking centrosome positioning behavior in different confinement conditions (Fig. S3 A, top). Cell polarity is also defined by the relative position of the nucleus with respect to the centrosome (Luxton and Gundersen, 2011), and in migrating cells, actin contractility regulates nuclear movements and orients the nuclear–centrosomal axis (Gomes et al., 2005). We quantified the distance between the centers of nuclei in micropatterned MDCK cells as a measure of relative nuclear positioning (Fig. 3 E). In different confinement conditions, lumen-initiating cells consistently exhibited larger internuclear distances (Fig. 3 G). These findings indicate that cell confinement controls the orientation of the nuclear–centrosomal axis and suggest that centrosomal positioning, by repositioning the vesicular trafficking machinery toward the cell junctions, is required for lumen initiation.

Myosin II inhibition suppresses peripheral actin contractility and induces centrosomal orientation and lumen initiation

Alterations in actin contractility, regulated by myosin II, constitute the main cellular response to changes in cell confinement and consequent cell spreading. Increased cell spreading (low confinement) results in augmented ventral actin polymerization and filament bundling (Pitaval et al., 2010). Accordingly, highly confined MDCK cells on collagen I micropatterns exhibited fewer stress fibers and decreased paxillin staining as compared with cells in low confinement conditions (Fig. 1 A and Fig. S1, A and B). On the other hand, it is well established that cortical actomyosin contractility controls the position of the centrosome

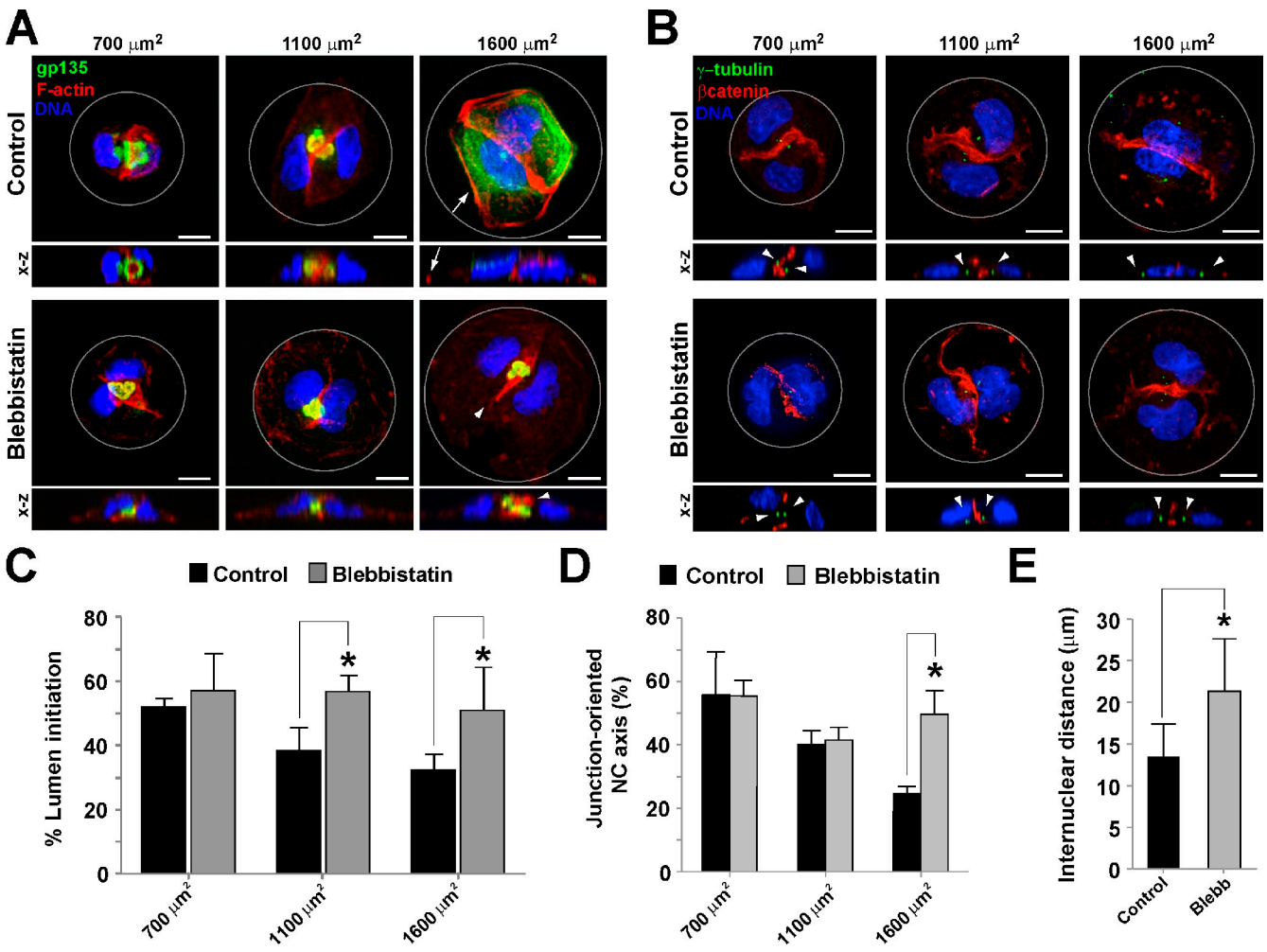

Figure 4. **Effect of myosin II inhibition on actin polarization, centrosome positioning, and lumen initiation.** (A) Effect of BB on lumen initiation. MDCK cells were seeded to grow cysts on collagen I–coated micropatterns of different sizes for 24 h. Cell cultures were treated with 50 µM BB for 30 min and then fixed and stained for F-actin, gp135, and nuclei. Cells were analyzed by confocal microscopy (z-stack projections are shown). Gray circles indicate pattern shape. An x-z view is shown for each image. Arrows indicate peripheral actin fibers. Arrowheads indicate junctional actin polarization and normal apical membrane formation. (B) Effect of BB on centrosome positioning. MDCK cells were seeded on micropatterns of different sizes, and cysts were grown for 24 h. Cell cultures were treated with 50 µM BB for 30 min and then fixed and stained for DNA, γ-tubulin, and β-catenin (red). Cells were analyzed by confocal microscopy (z-stack projections are shown). Gray circles indicate pattern shape. An x-z cross section is shown for each image. Arrowheads indicate centrosome localization. (C) Quantification of BB effect on lumen initiation. (D) Quantification of BB effect on centrosome positioning. NC, nucleus–centrosome. (E) Quantification of BB effect on internuclear distance in 1,600-µm² micropatterns. Values are means ± SD from three independent experiments ($n \geq 30$ cysts/experiment; *, $P < 0.005$). Bars, 10 µm.

in different animal species during both interphase and cell division (Bornens et al., 1989; Burakov et al., 2003; Gomes et al., 2005; Théry et al., 2005; Paluch et al., 2006; Fink et al., 2011). We thus investigated whether inhibition of actin contractility affected lumen initiation on micropatterns. Treatment of 3D micropatterned MDCK cells with the myosin II inhibitor blebbistatin (BB) suppressed actin contractility. Indeed, BB-treated cells exhibited a significant reduction in peripheral actin fibers, indicating that these structures are myosin II dependent (actomyosin II), but had no effect on junctional actin (Fig. 4 A, arrows and arrowheads). BB treatment of cells in low confinement conditions significantly rescued lumen initiation (Fig. 4 A). This result indicates that peripheral actomyosin II contractility in low confinement conditions prevents lumen initiation. To analyze the effect of BB on centrosome positioning, we stained cells for the centrosome marker γ-tubulin (Fig. 4 B). BB treatment of cells in low confinement conditions rectified centrosome orientation toward the cell junctions (Fig. 4, C and D), normal Golgi localization (Fig. S3 A, bottom), and nuclear positioning (Fig. 4, A, B, and E). These results suggest that low confinement conditions promote cell spreading and peripheral actomyosin II contractility, which may prevent the nuclear–centrosomal orientation required for lumen initiation. Inhibition of myosin II could be sufficient to correctly position the centrosome and initiate lumen formation.

Alternatively, increased cellular confinement may favor the formation or maintenance of cell–cell junctions that would then trigger centrosome repositioning and lumen initiation toward this compartment. To address this possibility, we analyzed the adherens junction markers β-catenin and E-cadherin and the focal adhesion marker vinculin in control and BB-treated cells attached to different-sized micropatterns (Fig. S3). Interestingly, we observed

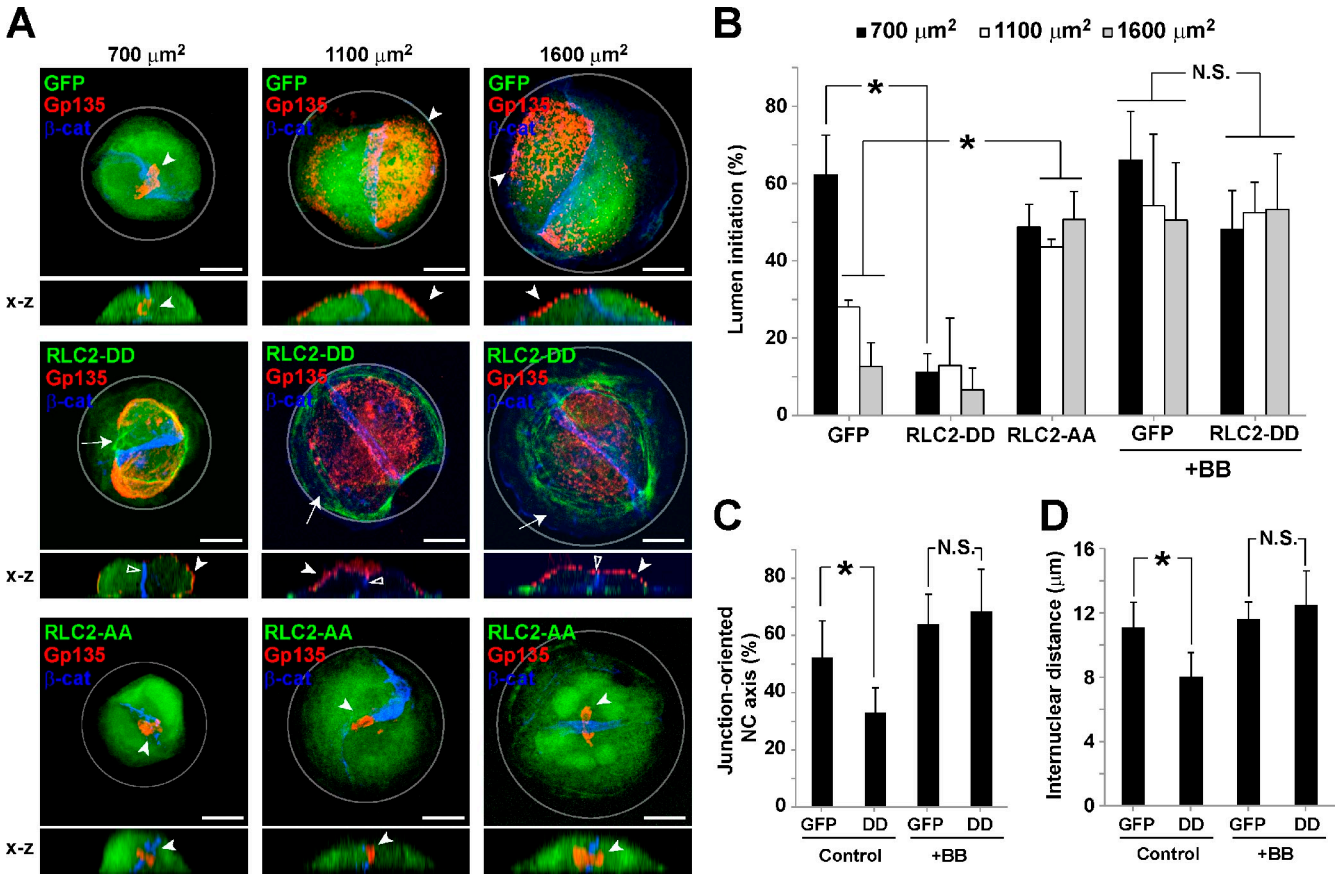

Figure 5. **Effect of myosin activation on lumen initiation.** (A) Effect of myosin RLC2 mutants (RLC2-DD and RLC2-AA) on lumen initiation. MDCK cells transfected with GFP-RLC2-DD, GFP-RLC2-AA, or GFP (control) were seeded on micropatterns of different sizes, and cysts were grown for 24 h. Cell cultures were fixed and stained for gp135 and β-catenin (β-cat). Cells were analyzed by confocal microscopy (z-stack projections are shown). Gray circles indicate pattern shape. An x-z view is shown for each image. Arrows indicate localization of RLC2-DD in peripheral contractile bundles. Filled arrowheads indicate apical membrane localization. Empty arrowheads indicate cell–cell junction position. Bars: (main images) 10 μm; (cross sections) 5 μm. (B) Quantification of RLC2-DD and RLC2-AA effects on lumen initiation. $n \geq 30$ cysts/experiment. (C) Quantification of RLC2-DD effect on centrosome positioning in high confinement (700 μm²). $n \geq 30$ cysts/experiment. NC, nucleus–centrosome. (D) Quantification of RLC2-DD effect on internuclear distance in high confinement (700 μm²). $n \geq 15$ cysts. Values are means ± SD from three independent experiments. *, $P < 0.05$.

similar distributions of β-catenin (Fig. S3, B and C, quantification) and E-cadherin (not depicted) in control and BB-treated cells in different confinement conditions. In contrast, vinculin was almost absent from cell–cell junctions and was mostly localized to peripheral focal adhesions, suggesting that these are the main tensile actin structures in micropatterned MDCK cells (Fig. S3 B, arrowheads). In fact, BB treatment disrupted peripheral vinculin staining, confirming the loss of peripheral contractility signaling (Fig. S3 B, bottom) but had no effect on vinculin levels at cellular junctions. Collectively, these results indicate that, in our experimental conditions, cell confinement does not significantly affect cell junction formation or maintenance, thus favoring the first possibility, in which nuclear–centrosomal orientation is modulated by peripheral actomyosin II contractility.

Constitutively active myosin II induces peripheral contractility and inhibits lumen initiation in conditions of high cell confinement

Myosin II activity is regulated by the myosin II regulatory light chain (RLC2), a subunit of the myosin II complex. The RLC2 subunit is phosphorylated by distinct protein kinases in two adjacent serine/threonine residues. Because the diphosphorylation of RLC2 activates the myosin II complex, expression of a double phosphomimetic RLC2 mutant, Thr-18-Asp/Ser-19-Asp (RLC2-DD), induces the formation of stable actin bundles and stress fibers in migrating cells (Vicente-Manzanares et al., 2008) and highly contractile structures in epithelial cells (Watanabe et al., 2007). RLC2-DD localized to peripheral bundles and stress fibers independently of cell confinement (Fig. 5 A, middle, arrows). Remarkably, cells expressing RLC2-DD formed significantly fewer lumens (Fig. 5, A [middle, arrowheads] and B [quantification]), and centrosome orientation was reduced in conditions of high confinement (Fig. 5 C). RLC2-DD expression also reduced internuclear distance (Fig. 5 D) but did not disrupt adherens junction formation (Fig. 5 A, middle, empty arrowheads). To confirm that cell confinement regulates lumen initiation specifically via myosin II activity, we treated RLC2-DD–transfected cells with BB, which significantly rescued lumen initiation (Fig. 5, B–D; and Fig. S3 D), and corrected centrosome orientation and nuclear positioning (Fig. 5, C and D). In contrast, overexpression of a nonphosphorylatable RLC2 mutant, Thr-18-Ala/Ser-19-Ala (RLC2-AA), produced similar effects to BB treatment in lumen initiation (Fig. 5 A, bottom;

and Fig. 4 B). Together, these findings indicate that low confinement increases cell spreading and peripheral contractility and inhibits lumen initiation and that inhibition of actomyosin II contractility is sufficient to restore centrosome positioning and initiate lumen morphogenesis.

An LKB1–RhoA pathway controls peripheral actin contractility in low confinement conditions

The Rho family GTPases are central regulators of cytoskeletal polarity and contractility (Heasman and Ridley, 2008). Different Rho-GTPases have been reported to activate myosin II via specific effectors, such as Rho kinase (ROCK) and myotonic dystrophy kinase–related Cdc42-binding kinase, which phosphorylate RLC2 (Wilkinson et al., 2005). In addition, Rho family GTPases control several steps associated with lumen formation (Martin-Belmonte et al., 2007; Ferrari et al., 2008; Yu et al., 2008; Strilić et al., 2009; Rodriguez-Fraticelli et al., 2010).

To analyze the contribution of the Rho–ROCK pathway to actomyosin II contractility during epithelial morphogenesis, we studied the effect of ROCK disruption on nuclear–centrosome positioning and lumen initiation in micropatterned MDCK cells. Treatment of cells with the ROCK inhibitor Y27632 resulted in a reduction in cortical stress fibers and significantly rescued normal lumen initiation and nuclear–centrosomal orientation in low confinement conditions (Fig. S4, A–C), thus mimicking the effects of BB treatment. These results indicate that peripheral actomyosin contractility is controlled by Rho–ROCK and that ROCK inhibition is sufficient to initiate lumen formation in conditions of low cell confinement.

Actin contractility is regulated by the master kinase Par-4/LKB1 both in culture (Williams and Brenman, 2008; Zagórska et al., 2010; Mirouse and Billaud, 2011) and in vivo (Chartier et al., 2011). Recent experiments have shown that LKB1 directly regulates RhoA–ROCK activation in epithelial cells (Xu et al., 2010) and centrosome positioning in neuronal cells (Asada et al., 2007). We thus analyzed the role of LKB1 in actin contractility and lumen formation in micropatterned cells. LKB1 localized to actin-rich intercellular junctions and peripheral actin structures in MDCK cells in both micropatterns and 3D cysts (Fig. S5, A and C), suggesting a role in actin contractility, consistent with a previous study (Sebbagh et al., 2009).

To analyze LKB1 function, we used a doxycycline (dox)-inducible MDCK cell line expressing small hairpin RNA (shRNA) for specific LKB1 silencing (Boehlke et al., 2010), which efficiently silenced LKB1 in dox-treated cells (Fig. S5 B). Interestingly, LKB1-silenced cells on micropatterns exhibited a significant decrease in peripheral F-actin staining in low cell confinement conditions (Fig. 6, A and B), which was sufficient to restore correct centrosome orientation (Fig. 6, C and E), lumen initiation, and nuclear positioning (Fig. 6, A–F). However, LKB1 function was required at later stages for normal cyst development (Fig. S5, D and E), consistent with previous studies that have characterized a role for LKB1 in apical junction formation (Hezel et al., 2008; Amin et al., 2009). To determine whether the effect of LKB1 on early lumen initiation was Rho dependent, we analyzed RhoA activity by pull-down assay, which revealed a 60% decrease in GTP-bound RhoA levels in LKB1-silenced cells in low confinement conditions (Fig. 6 G). Furthermore, in LKB1-silenced cells, expression of constitutively active RhoA (RhoA-V14) inhibited lumen initiation, whereas treatment with ROCK inhibitor had no further effect on lumen initiation (Fig. 6, H and I), confirming that RhoA lies downstream of LKB1 in this pathway. Collectively, these results indicate that in low confinement conditions, LKB1 activity regulates RhoA–ROCK-mediated actomyosin contractility, which in turn impairs normal centrosome positioning and lumen initiation.

Disruption of aPKC impairs centrosome positioning and lumen initiation independent of cell confinement or contractility

Our data indicate that cell confinement modulates centrosome position, which localize near the cell junctions to form the lumen in permissive conditions. These observations could be compatible with the existence of specific machinery to maintain the positioning of centrosome at the cell junction, independent of cell confinement or actin contractility. In that case, the disruption of this machinery should inhibit lumen initiation independent of cell confinement or actin contractility. To test this hypothesis, we targeted the Par6–atypical PKC (aPKC) complex, which is an important regulator of centrosome orientation and is required for lumen formation (Etienne-Manneville and Hall, 2003; Etienne-Manneville et al., 2005; Manneville and Etienne-Manneville, 2006; Martin-Belmonte et al., 2007). We found that in low confinement conditions, active aPKC (phosphorylated aPKC) was localized at cell–cell junctions in both normal and BB-treated cells (Fig. 7 A). Inhibition of aPKC activity using a myristoylated pseudosubstrate (PS) aPKC inhibitor (aPKC-PS) reduced lumen initiation and disrupted centrosome positioning both in conditions of high or low confinement (Fig. 7, B–D). BB treatment was not sufficient to rescue centrosome positioning or lumen formation in aPKC-PS–treated cells in either low or high confinement conditions (Fig. 7, B–D), implying that positioning of the centrosome at the cell junctions depends on aPKC activity independent of actin contractility. Thus, our data indicate that aPKC activity is required to properly position the centrosome at the cell junction during lumen initiation and suggest that centrosome positioning is required for lumen initiation. Interestingly, internuclear distance was significantly increased in cells treated with BB and aPKC-PS, indicating that nuclear positioning is regulated by actomyosin II, but not by aPKC, and suggesting that nuclear positioning and centrosome positioning might be regulated differently during lumen initiation in 3D MDCK cells (Fig. 7, E and F). In summary, our data indicate that aPKC activity is required to keep the centrosome in proper position during lumen initiation.

Discussion

In the present study, we characterized the role of cell confinement in lumen formation using a new methodology to analyze 3D epithelial morphogenesis in micropatterns. We found that

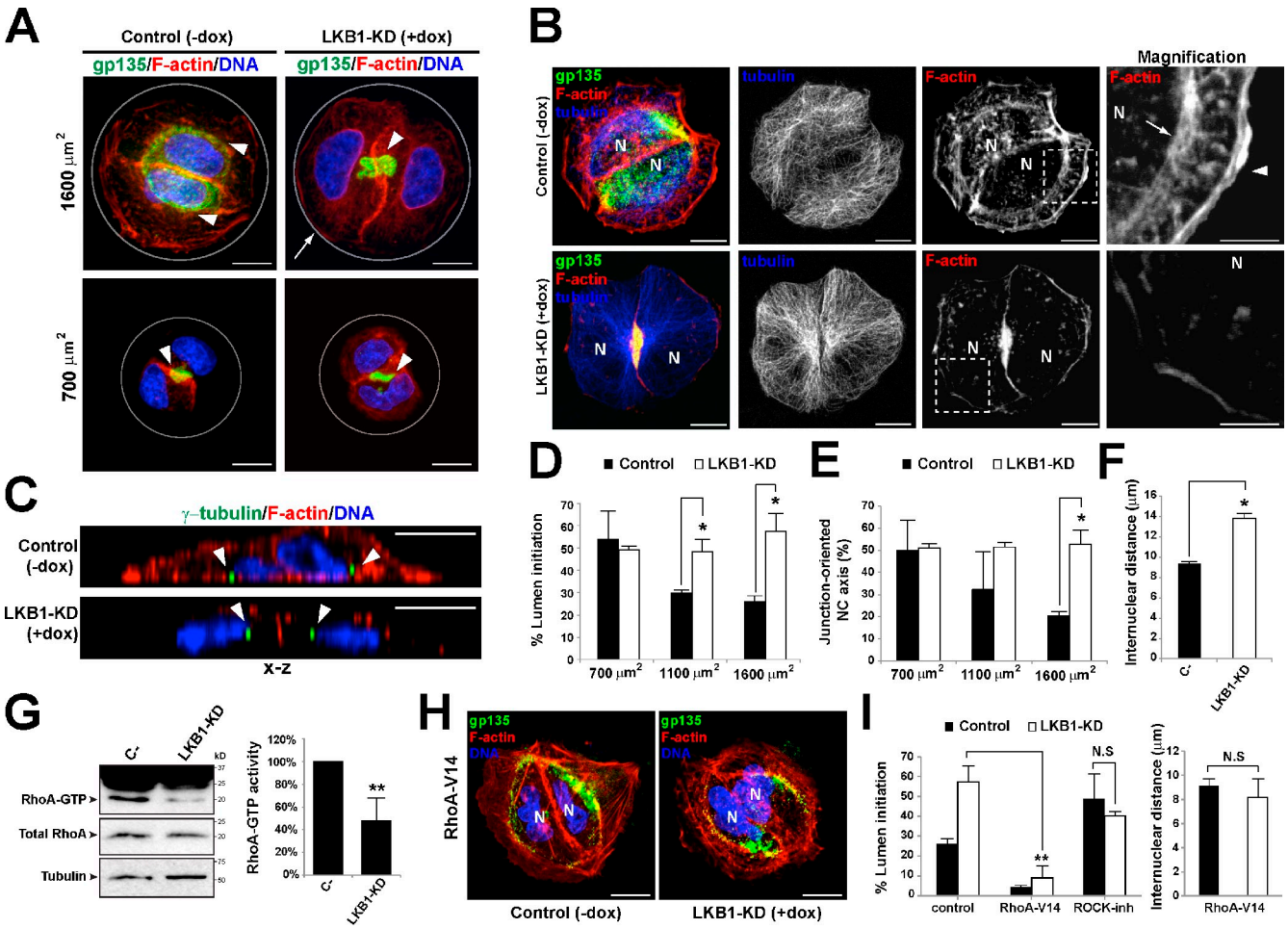

Figure 6. **LKB1 controls peripheral actin contractility through RhoA activation.** (A) Effect of LKB1 silencing in lumen initiation in micropatterned cysts. Control cells (−dox) or LKB1-KD (+dox) cells were seeded on micropatterns of different sizes and grown to form cysts. Micropatterned cells were fixed at 24 h and stained for gp135, F-actin, and nuclei. Gray circles indicate pattern shape. Arrowheads show apical membrane. Arrow shows reduced peripheral actin staining. (B) Effect of LKB1-KD in actin and microtubule cytoskeleton. Control cells (−dox) or LKB1-KD (+dox) cells on collagen-coated 1,600-μm² micropatterns were stained for gp135, F-actin, and tubulin. N, nuclei. Arrow indicates subcortical actin stress fibers. Arrowheads indicate cortical actin fibers. (C) Effect of LKB1-KD in centrosome positioning. Control cells (−dox) or LKB1-KD (+dox) cells grown to form cysts on collagen-coated 1,600-μm² micropatterns were fixed after 24 h. Cells were stained for γ-tubulin, F-actin, and DNA. An x-z cross section of cell doublets is shown. Arrowheads indicate centrosome position. (D) Quantification of correct lumen initiation in LKB1-KD cells. Control cells (−dox) or LKB1-KD (+dox) cysts fixed at 24 h were stained for gp135, F-actin, and nuclei. $n \geq 50$ cysts/experiment. (E) Quantification of centrosome position in LKB1-KD cells. $n \geq 50$ cysts/experiment. (F) Quantification of internuclear distance in LKB1-KD cells. $n \geq 50$ cysts/experiment. (G) RhoA-GTP levels in LKB1-KD cells. Control (C−) or LKB1-KD cells cultured at low density on collagen I–treated dishes were lysed, and RhoA-GTP levels were analyzed by pull-down assay using GST-tagged Rhotekin Rho-binding domain. Band intensity was quantified from three different experiments. Values are mean percentages of control ± SD (**, $P < 0.001$). (H) Effect of RhoA-V14 expression in LKB1-KD cells. Control or LKB1-KD cells transfected with RhoA-V14 were seeded on circular 1,600-μm² micropatterns to grow cysts and fixed after 24 h. Cysts were stained for gp135, F-actin, and tubulin. N, nuclei. (I) Quantification of lumen initiation and internuclear distances in RhoA-V14–expressing and ROCK-inhibited (inh) LKB1-KD cells. $n \geq 30$ cysts/experiment; **, $P < 0.005$. Values are means ± SD from three independent experiments. *, $P < 0.005$. Bars, 10 μm.

cell confinement, which modifies the actomyosin II–mediated contractility, is able to regulate epithelial polarity and lumen formation and the positioning of the centrosome and the nucleus. In conditions of low confinement, cell spreading increases peripheral actin contractility, which in turn impairs the initiation of lumen formation. Peripheral actomyosin contractility maintains centrosome positioning at the center of the cell perimeter and forces nuclear positioning toward the cell–cell junctions (Fig. 8). In contrast, in highly confined cells, peripheral actomyosin contractility is suppressed, allowing centrosome positioning toward the junctional membrane compartment and lumen initiation between adjacent cells (Fig. 8). Interestingly, laminin-rich ECMs inhibited cell spreading, recreating high confinement conditions and improving lumen formation outcomes. Supporting this hypothesis, myosin II inhibition induced lumen initiation on lowly confined cells, whereas expression of constitutively diphosphorylated RLC2 (RLC2-DD), an active form of myosin II, suppressed lumen initiation on high confinement. On the other hand, we observed that the activity of the aPKC signaling pathway at cellular junctions mediates centrosome relocation independent of cell confinement, consistent with previous studies (Georgiou et al., 2008; Desai et al., 2009; Wallace et al., 2010). In summary, these data suggest that the balance between the pathways controlling peripheral and junctional actin-stabilized compartments regulates centrosome positioning and initiation of epithelial morphogenesis (Fig. 8).

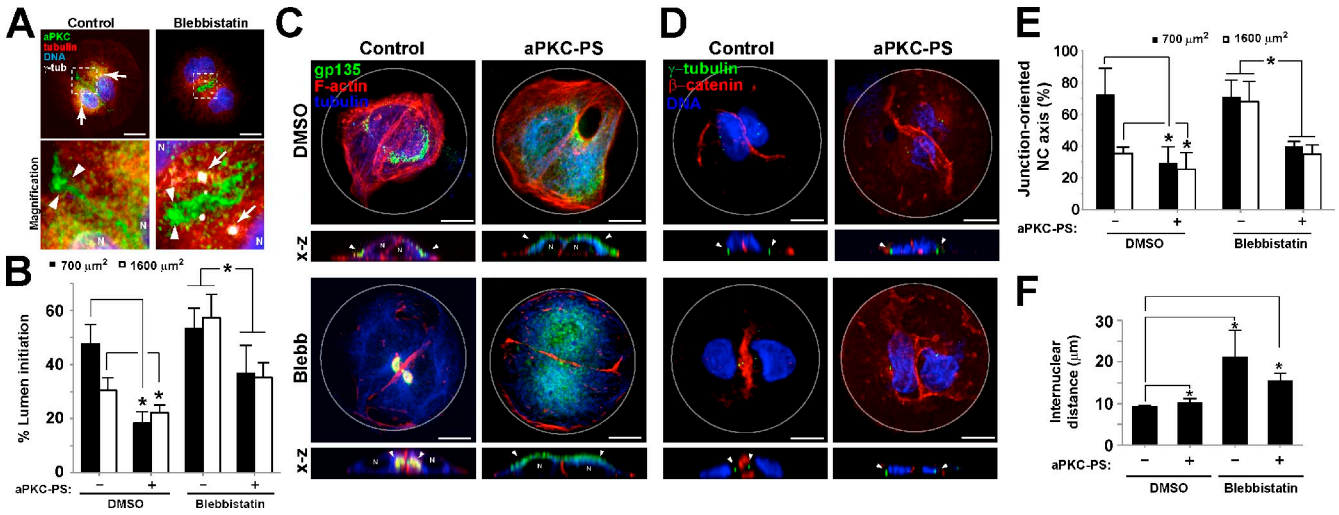

Figure 7. **Nuclear–centrosomal orientation during lumen initiation requires aPKC.** (A) Localization of aPKC in control or BB-treated MDCK cells. MDCK cells were seeded on micropatterns and treated with BB. Cells were fixed and stained to detect aPKC, tubulin, nuclei (blue), and γ-tubulin (γ-tub; gray). Arrowheads indicate aPKC localization at lateral plasma membrane. Arrows indicate centrosome localization. Dotted boxes show areas of magnification. (B) Quantification of lumen initiation in aPKC-PS inhibitor-treated cells. $n \geq 50$ cysts/experiment. (C) Effect of aPKC inhibition in BB (Bleb)-induced lumen morphogenesis on low confinement. MDCK cells were seeded on 1,600-μm² collagen I micropatterns and treated with 40 μg/ml aPKC-PS overnight. After 24 h, cells were treated with BB for 45 min and then were fixed and stained to detect gp135, F-actin, and tubulin. Cells were analyzed by confocal microscopy (z-stack projections and x-z cross sections are shown). Arrowheads show apical membrane. (D) Effect of aPKC inhibition on centrosome positioning. Cells grown as in C were fixed and stained to detect γ-tubulin, β-catenin, and DNA. Cells were analyzed by confocal microscopy (z-stack projections and x-z cross sections are shown). Gray circles indicate pattern shape. Arrowheads show centrosome position. (E) Quantification of centrosome positioning in aPKC inhibitor–treated cells. $n \geq 30$ cysts/experiment. NC, nucleus–centrosome. (F) Quantification of internuclear distance in aPKC inhibitor–treated cells. $n \geq 30$ cysts/experiment. Values are means ± SD from three independent experiments. *, $P < 0.05$. N, nuclei. Bars, 10 μm.

Centrosome positioning to specific regions close to the plasma membrane is considered essential for protein trafficking processes, such as the delivery of secretory granules to the immunological synapse in cytotoxic T lymphocytes, and for axon formation during the development of neuronal polarity (de Anda et al., 2005; Stinchcombe et al., 2006). Similarly, proper centrosome positioning could be critical to position the vesicular trafficking machinery for normal lumen formation. However, the role of centrosome positioning in epithelial lumen formation has not been clearly established. Our findings reveal that aPKC is required for centrosome positioning and lumen initiation independent of actin contractility, suggesting that centrosome positioning is required to initiate the lumen, but further studies will be required to clearly demonstrate this mechanism. Lumen initiation requires the activation of small GTPases, such as Cdc42, Rab8, Rab11, and the exocyst (Martin-Belmonte et al., 2007; Sfakianos et al., 2007; Schlüter et al., 2009; Bryant et al., 2010). Notably, Cdc42 guanine nucleotide exchange factors (GEFs; ITSN2) and Rab8 GEFs (Rabin8) localize at the centrosome in MDCK cells (Bryant et al., 2010; Rodriguez-Fraticelli et al., 2010). This suggests that centrosome positioning could potentially define Rab8 and Cdc42 activation in target plasma membrane compartments during lumen formation.

In accordance with previous studies in migrating cells, actomyosin II contractility also affected the position of the nuclei (Gomes et al., 2005; Luxton and Gundersen, 2011). Peripheral contractility actively localizes nuclei to the center of the cell aggregate, precluding nuclear–centrosomal axis orientation to form the lumen. When peripheral actin contractility is reduced, nuclear positioning appears to facilitate polarity reorientation and lumen initiation. In this respect, cells in low confinement conditions mimic the behavior of cells in wound closure assays, which produce contractile actin at the wound edge that repels the nuclei from the wound to orient the nuclear–centrosomal axis (Gomes et al., 2005). However, it remains unclear whether nuclear positioning in epithelial cells is controlled directly by nuclear membrane actin-binding proteins (Luxton et al., 2010).

Our results also demonstrate that the tumor suppressor kinase LKB1 and the RhoA signaling pathway regulate peripheral actomyosin II–mediated contractility. LKB1 control of myosin II activity through RLC2 phosphorylation has been previously described, although there is some controversy as to how this effect is directly mediated downstream of LKB1 (Mirouse et al., 2007; Zagórska et al., 2010; Chartier et al., 2011). Furthermore, LKB1 overexpression has been shown to control RhoA activity through the activation of a RhoGEF (Xu et al., 2010), which may result in ROCK activation. Our results suggest that LKB1 pathways activate RhoA–ROCK-mediated contractility in the basal compartment, preventing lumen initiation when the conditions of confinement are inappropriate. However, epithelial cells also require LKB1 and Rho–ROCK activity to stabilize the cell–cell junctions and maintain epithelial polarity (Mirouse et al., 2007). Consistent with this, disruption of the LKB1–Rho–ROCK–myosin pathway for longer periods after lumen initiation abolishes lumen expansion and normal epithelial morphogenesis (Fig. S5; Ferrari et al., 2008). Epithelial cells therefore need to finely control the mechanisms that regulate contractility and confinement to preserve the polarized phenotype. In fact, aggressive epithelial cancer cells, which frequently harbor mutations in LKB1 or Rho-GTPase signaling

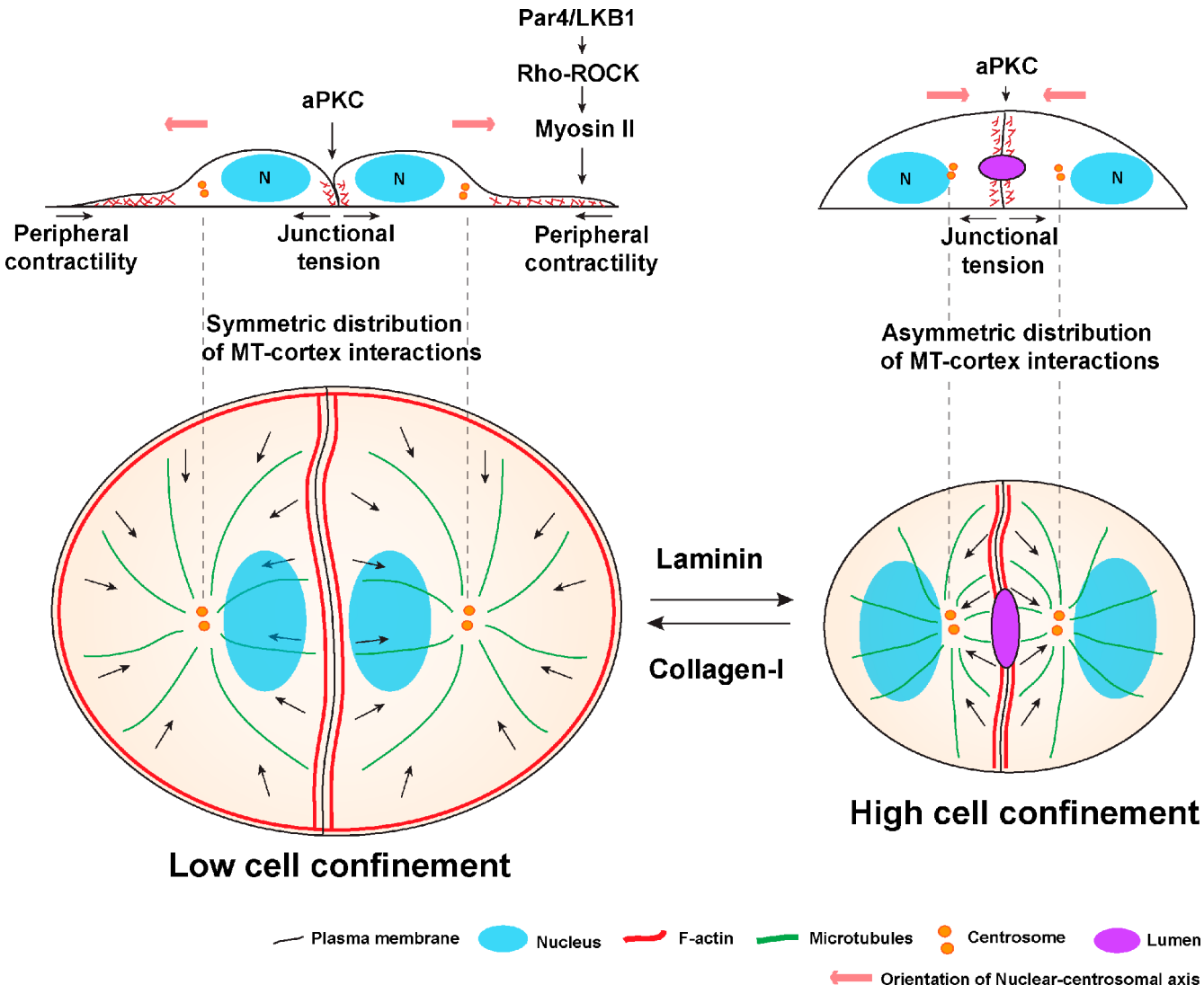

Figure 8. **Model for cell confinement regulation of lumen morphogenesis.** In highly adhesive substrates, such as collagen I, low cell confinement induces cell spreading, promoting formation of peripheral nuclear and cortical actin fibers and maintaining the centrosome positioned at the cell center and nuclei close to the junctions. Cell confinement prevents cell spreading, contractility is reduced, and centrosomes reposition toward the cell junctions where the initial lumen forms. Peripheral actin contractility depends on LKB1-mediated regulation of myosin II activity through Rho–ROCK, whereas contractility-independent centrosome positioning is controlled by aPKC activity at the junctions. MT, microtubule; N, nuclei.

components, exhibit increased cell migration and invasion capabilities (Butcher et al., 2009; Samuel et al., 2011). Further studies are required to clarify the role of LKB1 and its relationship with Rho-mediated contractility in cell polarity and cancer initiation and progression.

Materials and methods

Cell culture

MDCK cells (NBL2 clone) were cultured using 10% fetal bovine serum–supplemented complete MEM, containing 50 µm/ml penicillin-streptomycin and 2 mM L-Gln (Gibco), and passaged according to American Type Culture Collection instructions. Stably transfected MDCK cells (Lifeact-GFP) were grown and maintained in 0.5 mg/ml G418 or 0.1 mg/ml hygromycin B. To grow cells on agar substrate, a cell culture–tested agar solution was incubated on coverslips, and cells were seeded at 40,000 cells/cm^2. For lumen initiation experiments, cells were cultured in the presence of 2% Matrigel (BD) to induce cyst morphogenesis. MDCK cells stably expressing Venus-LKB1 and pLV-shLKB1 were gifts from the G. Walz laboratory (University of Freiburg, Freiburg, Germany; Boehlke et al., 2010).

Micropatterned cell culture

MDCK cells were cultured on micropatterned CYTOOchips using proprietary technology obtained from CYTOO, Inc. Disk-shaped micropatterns of different surface area size were used for most experiments (small = 700 µm^2; medium = 1,100 µm^2; large = 1,600 µm^2). Cells were seeded at 20,000 cells/ml (80,000 cells/chip) in complete MEM and then washed and incubated according to the manufacturer's instructions.

Plasmids, reagents, antibodies, and inhibitors

Life-actin probe cDNA was cloned into the pEGFP-N1 vector. pEGFP-C1-RhoV14 was a gift from I. Correas (Universidad Autónoma de Madrid, Madrid, Spain). pEGFP-C1-RLC2 mutants were gifts from M. Vicente-Manzanares (Universidad Autónoma de Madrid, Madrid, Spain). For ECM coating, CYTOOchips were incubated with collagen I (from rat tail; Sigma-Aldrich) or laminin (from ECM extracts; Sigma-Aldrich) at 20 µg/ml for 1 h and washed twice with 20 ml PBS before use. Antibodies used were gp135/podocalyxin (1:5,000, 3B8; gift from G. Ojakian, State University of New York Downstate Medical Center, New York, NY), α-tubulin (1:2,000, DM1A [Sigma-Aldrich]; 1:1,000, YL1/2 [gift from J. Kilmartin, Medical Research Council, Cambridge, England, UK]), γ-tubulin (1:1,000, GT-88; Sigma-Aldrich), β-catenin (1:1,000; Santa Cruz Biotechnology, Inc.), paxillin (1:1,000; BD), vinculin (1:1,000; BD), RhoA (1:1,000; BD),

and p-PKC-ζ (Thr410; 1:500, sc-12894; Santa Cruz Biotechnology, Inc.). Phalloidin-FITC and -TRITC were used to stain F-actin (1:5,000), and DAPI (1:1,000), Hoechst 33842 (1:10,000), and Topro-3 (1:500) were used to stain nuclei (Molecular Probes; Invitrogen). MDCK cells were treated with 40 µg/ml aPKC-PS (EMD Millipore), 50 µM BB (Sigma-Aldrich), or 20 µM Y27632 (Sigma-Aldrich) at the indicated times. Dox (Sigma-Aldrich) was used for inducible expression plasmids (0.1 µg/ml).

RNAi

The LKB1-targeting shRNA for MDCK cells was previously characterized (Boehlke et al., 2010). Inducible LKB1 silencing was verified by quantitative RT-PCR using specific primers (forward, 5′-CTGAGGAGATTACGGCACAA-3′; and reverse, 5′-CGCAGTACTCCATCACCATATA-3′).

Immunofluorescence and quantifications

MDCK cells were fixed at different time points and stained by immunofluorescence using the indicated primary antibodies. Pacific blue (405)– or Alexa Fluor 488/555/647–conjugated anti–rabbit and anti–mouse were used as secondary antibodies (Life Technologies). Images were acquired using inverted/vertical confocal microscopes (LSM 510 or LSM 710; Carl Zeiss) using the ZEN software (Carl Zeiss). Objectives used were 63×/NA 1.4 oil Plan Apochromat and 100×/NA 1.4 oil Plan Apochromat (Carl Zeiss). Then, images were treated using ImageJ software (National Institutes of Health) for producing x-z orthogonal slices, z-stack projections, and 3D deconvolution. For quantifications, more than three experiments were quantified (analyzing ∼50 cells per condition) using different CYTOOchips. Accumulation of a gp135 after 24 h in a single membrane patch at cell–cell junctions was used to quantify normal initiating lumens. For centrosome positioning, we analyzed the angle between the two nuclei and γ-tubulin staining to determine the position of the centrosome. Centrosomes oriented within 90° from the nuclei–nuclei axis were considered to be correctly oriented toward the cell–cell junctions. Significance was calculated using a paired, two-tailed Student's *t* test, and significant p-values are indicated in each experiment.

Rho-GTP pull-down experiments

In brief, cells plated at low confluence (10,000 cells/ml) on collagen-coated 10-cm dishes were lysed using TBS (1% Triton X-100 and 0.1% SDS) with 25 mM $MgCl_2$ and protease inhibitors. Lysates were loaded with Sepharose-glutathione beads bound to the purified Rhotekin-binding domain and 100 µg/ml lysate, incubated for 20 min (4°C), and washed twice with lysis buffer. Beads were dried by aspiration, and bound protein was eluted with 50 µl Laemmli loading buffer (95°C). Band intensity in a Western blot was quantified by optical densitometry (ImageJ).

Live-cell imaging

For live-cell imaging, MDCK cells were seeded on CYTOOchips and incubated in CYTOOchambers for different times, according to manufacturer's instructions. Live imaging experiments were performed using incubator chamber accessories for each system at 37°C and 5% CO_2. Imaging medium was red-free complete MEM (Life Technologies) supplemented with 2% Matrigel. Images were acquired with a 63×/NA 1.2 oil immersion objective using a video microscope (Eclipse Ti; Nikon) or with a 40×/NA 0.60 dry objective using a microscope (AF6000 LX [Leica]; camera [885 EM; Andor]). MetaMorph software (Nikon) or Leica Application Suite (Leica) was used for acquisition and video analysis.

Online supplemental material

Fig. S1 shows focal adhesions, Golgi apparatus, and tight junction stainings in micropatterned cysts and laminin distribution in different confinement conditions at 24 h. Fig. S2 shows that cell confinement controls time of lumen initiation and centrosome positioning but not spindle orientation in cell division. Fig. S3 shows the myosin II inhibition effects on Golgi polarization and vinculin staining. Fig. S4 shows that ROCK inhibition mimics BB effects on micropatterned cysts. Fig. S5 shows the LKB1-knockdown (KD) phenotype in mature MDCK cysts. Video 1 shows MDCK cyst formation in micropatterns using wide-field light microscopy. Video 2 shows Life-actin GFP staining of a micropatterned MDCK cyst growing in high confinement conditions. Video 3 shows Life-actin GFP staining of a micropatterned MDCK cyst growing in low confinement conditions. Online supplemental material is available at http://www.jcb.org/cgi/content/full/jcb.201203075/DC1.

We thank Carmen M. Ruiz-Jarabo for comments on the manuscript and members of the Alonso and Martin-Belmonte laboratory for discussion. We thank Miguel Vicente-Manzanares for RLC2-(T18D,S19D) plasmids and reagents and George Ojakian for the gp135/podocalyxin antibody.

This work was supported by grants from the Human Frontiers Science Program (Human Frontiers Science Program Career Development Award 00011/2009), Marie Curie (IRG-209382), Ministerio de Ciencia e Innovación (BFU2008-01916 and BFU2011-22622), and CONSOLIDER (CSD2009-00016) to F. Martín-Belmonte. A.E. Rodríguez-Fraticelli is the recipient of a Junta para la Ampliación de Estudios fellowship from Consejo Superior de Investigaciones Científicas. An institutional grant from Fundación Ramón Areces to Centro de Biología Molecular Severo Ochoa is also acknowledged.

Submitted: 15 March 2012
Accepted: 16 August 2012

References

Amin, N., A. Khan, D. St Johnston, I. Tomlinson, S. Martin, J. Brenman, and H. McNeill. 2009. LKB1 regulates polarity remodeling and adherens junction formation in the *Drosophila* eye. *Proc. Natl. Acad. Sci. USA*. 106:8941–8946. http://dx.doi.org/10.1073/pnas.0812469106

Asada, N., K. Sanada, and Y. Fukada. 2007. LKB1 regulates neuronal migration and neuronal differentiation in the developing neocortex through centrosomal positioning. *J. Neurosci.* 27:11769–11775. http://dx.doi.org/10.1523/JNEUROSCI.1938-07.2007

Boehlke, C., F. Kotsis, V. Patel, S. Braeg, H. Voelker, S. Bredt, T. Beyer, H. Janusch, C. Hamann, M. Gödel, et al. 2010. Primary cilia regulate mTORC1 activity and cell size through Lkb1. *Nat. Cell Biol.* 12:1115–1122. http://dx.doi.org/10.1038/ncb2117

Bornens, M. 2012. The centrosome in cells and organisms. *Science*. 335:422–426. http://dx.doi.org/10.1126/science.1209037

Bornens, M., M. Paintrand, and C. Celati. 1989. The cortical microfilament system of lymphoblasts displays a periodic oscillatory activity in the absence of microtubules: implications for cell polarity. *J. Cell Biol.* 109:1071–1083. http://dx.doi.org/10.1083/jcb.109.3.1071

Bryant, D.M., and K.E. Mostov. 2008. From cells to organs: building polarized tissue. *Nat. Rev. Mol. Cell Biol.* 9:887–901. http://dx.doi.org/10.1038/nrm2523

Bryant, D.M., A. Datta, A.E. Rodríguez-Fraticelli, J. Peränen, F. Martín-Belmonte, and K.E. Mostov. 2010. A molecular network for de novo generation of the apical surface and lumen. *Nat. Cell Biol.* 12:1035–1045. http://dx.doi.org/10.1038/ncb2106

Burakov, A., E. Nadezhdina, B. Slepchenko, and V. Rodionov. 2003. Centrosome positioning in interphase cells. *J. Cell Biol.* 162:963–969. http://dx.doi.org/10.1083/jcb.200305082

Butcher, D.T., T. Alliston, and V.M. Weaver. 2009. A tense situation: forcing tumour progression. *Nat. Rev. Cancer*. 9:108–122. http://dx.doi.org/10.1038/nrc2544

Chartier, N.T., D.P. Salazar Ospina, L. Benkemoun, M. Mayer, S.W. Grill, A.S. Maddox, and J.C. Labbé. 2011. PAR-4/LKB1 mobilizes nonmuscle myosin through anillin to regulate *C. elegans* embryonic polarization and cytokinesis. *Curr. Biol.* 21:259–269. http://dx.doi.org/10.1016/j.cub.2011.01.010

Datta, A., D.M. Bryant, and K.E. Mostov. 2011. Molecular regulation of lumen morphogenesis. *Curr. Biol.* 21:R126–R136. http://dx.doi.org/10.1016/j.cub.2010.12.003

de Anda, F.C., G. Pollarolo, J.S. Da Silva, P.G. Camoletto, F. Feiguin, and C.G. Dotti. 2005. Centrosome localization determines neuronal polarity. *Nature*. 436:704–708. http://dx.doi.org/10.1038/nature03811

Desai, R.A., L. Gao, S. Raghavan, W.F. Liu, and C.S. Chen. 2009. Cell polarity triggered by cell-cell adhesion via E-cadherin. *J. Cell Sci.* 122:905–911. http://dx.doi.org/10.1242/jcs.028183

Discher, D.E., P. Janmey, and Y.L. Wang. 2005. Tissue cells feel and respond to the stiffness of their substrate. *Science*. 310:1139–1143. http://dx.doi.org/10.1126/science.1116995

DuFort, C.C., M.J. Paszek, and V.M. Weaver. 2011. Balancing forces: architectural control of mechanotransduction. *Nat. Rev. Mol. Cell Biol.* 12:308–319. http://dx.doi.org/10.1038/nrm3112

Etienne-Manneville, S., and A. Hall. 2003. Cdc42 regulates GSK-3beta and adenomatous polyposis coli to control cell polarity. *Nature*. 421:753–756. http://dx.doi.org/10.1038/nature01423

Etienne-Manneville, S., J.B. Manneville, S. Nicholls, M.A. Ferenczi, and A. Hall. 2005. Cdc42 and Par6–PKCζ regulate the spatially localized association of Dlg1 and APC to control cell polarization. *J. Cell Biol.* 170:895–901. http://dx.doi.org/10.1083/jcb.200412172

Ferrari, A., A. Veligodskiy, U. Berge, M.S. Lucas, and R. Kroschewski. 2008. ROCK-mediated contractility, tight junctions and channels contribute to the conversion of a preapical patch into apical surface during isochoric lumen initiation. *J. Cell Sci.* 121:3649–3663. http://dx.doi.org/10.1242/jcs.018648

Fink, J., N. Carpi, T. Betz, A. Bétard, M. Chebah, A. Azioune, M. Bornens, C. Sykes, L. Fetler, D. Cuvelier, and M. Piel. 2011. External forces control mitotic spindle positioning. *Nat. Cell Biol.* 13:771–778. http://dx.doi.org/10.1038/ncb2269

Georgiou, M., E. Marinari, J. Burden, and B. Baum. 2008. Cdc42, Par6, and aPKC regulate Arp2/3-mediated endocytosis to control local adherens junction stability. *Curr. Biol.* 18:1631–1638. http://dx.doi.org/10.1016/j.cub.2008.09.029

Gomes, E.R., S. Jani, and G.G. Gundersen. 2005. Nuclear movement regulated by Cdc42, MRCK, myosin, and actin flow establishes MTOC polarization in migrating cells. *Cell*. 121:451–463. http://dx.doi.org/10.1016/j.cell.2005.02.022

Heasman, S.J., and A.J. Ridley. 2008. Mammalian Rho GTPases: new insights into their functions from in vivo studies. *Nat. Rev. Mol. Cell Biol.* 9:690–701. http://dx.doi.org/10.1038/nrm2476

Hezel, A.F., S. Gurumurthy, Z. Granot, A. Swisa, G.C. Chu, G. Bailey, Y. Dor, N. Bardeesy, and R.A. Depinho. 2008. Pancreatic LKB1 deletion leads to acinar polarity defects and cystic neoplasms. *Mol. Cell. Biol.* 28:2414–2425. http://dx.doi.org/10.1128/MCB.01621-07

Jaffe, A.B., N. Kaji, J. Durgan, and A. Hall. 2008. Cdc42 controls spindle orientation to position the apical surface during epithelial morphogenesis. *J. Cell Biol.* 183:625–633. http://dx.doi.org/10.1083/jcb.200807121

Li, R., and G.G. Gundersen. 2008. Beyond polymer polarity: how the cytoskeleton builds a polarized cell. *Nat. Rev. Mol. Cell Biol.* 9:860–873. http://dx.doi.org/10.1038/nrm2522

Luxton, G.W., and G.G. Gundersen. 2011. Orientation and function of the nuclear-centrosomal axis during cell migration. *Curr. Opin. Cell Biol.* 23:579–588. http://dx.doi.org/10.1016/j.ceb.2011.08.001

Luxton, G.W., E.R. Gomes, E.S. Folker, E. Vintinner, and G.G. Gundersen. 2010. Linear arrays of nuclear envelope proteins harness retrograde actin flow for nuclear movement. *Science*. 329:956–959. http://dx.doi.org/10.1126/science.1189072

Manneville, J.B., and S. Etienne-Manneville. 2006. Positioning centrosomes and spindle poles: looking at the periphery to find the centre. *Biol. Cell*. 98:557–565. http://dx.doi.org/10.1042/BC20060017

Martin-Belmonte, F., A. Gassama, A. Datta, W. Yu, U. Rescher, V. Gerke, and K. Mostov. 2007. PTEN-mediated apical segregation of phosphoinositides controls epithelial morphogenesis through Cdc42. *Cell*. 128:383–397. http://dx.doi.org/10.1016/j.cell.2006.11.051

Mirouse, V., and M. Billaud. 2011. The LKB1/AMPK polarity pathway. *FEBS Lett.* 585:981–985. http://dx.doi.org/10.1016/j.febslet.2010.12.025

Mirouse, V., L.L. Swick, N. Kazgan, D. St Johnston, and J.E. Brenman. 2007. LKB1 and AMPK maintain epithelial cell polarity under energetic stress. *J. Cell Biol.* 177:387–392. http://dx.doi.org/10.1083/jcb.200702053

O'Brien, L.E., T.S. Jou, A.L. Pollack, Q. Zhang, S.H. Hansen, P. Yurchenco, and K.E. Mostov. 2001. Rac1 orientates epithelial apical polarity through effects on basolateral laminin assembly. *Nat. Cell Biol.* 3:831–838. http://dx.doi.org/10.1038/ncb0901-831

Ojakian, G.K., W.J. Nelson, and K.A. Beck. 1997. Mechanisms for de novo biogenesis of an apical membrane compartment in groups of simple epithelial cells surrounded by extracellular matrix. *J. Cell Sci.* 110: 2781–2794.

Paluch, E., J. van der Gucht, and C. Sykes. 2006. Cracking up: symmetry breaking in cellular systems. *J. Cell Biol.* 175:687–692. http://dx.doi.org/10.1083/jcb.200607159

Pitaval, A., Q. Tseng, M. Bornens, and M. Théry. 2010. Cell shape and contractility regulate ciliogenesis in cell cycle–arrested cells. *J. Cell Biol.* 191:303–312. http://dx.doi.org/10.1083/jcb.201004003

Rodriguez-Fraticelli, A.E., S. Vergarajauregui, D.J. Eastburn, A. Datta, M.A. Alonso, K. Mostov, and F. Martín-Belmonte. 2010. The Cdc42 GEF Intersectin 2 controls mitotic spindle orientation to form the lumen during epithelial morphogenesis. *J. Cell Biol.* 189:725–738. http://dx.doi.org/10.1083/jcb.201002047

Rodríguez-Fraticelli, A.E., M. Gálvez-Santisteban, and F. Martín-Belmonte. 2011. Divide and polarize: recent advances in the molecular mechanism regulating epithelial tubulogenesis. *Curr. Opin. Cell Biol.* 23:638–646. http://dx.doi.org/10.1016/j.ceb.2011.07.002

Samuel, M.S., J.I. Lopez, E.J. McGhee, D.R. Croft, D. Strachan, P. Timpson, J. Munro, E. Schröder, J. Zhou, V.G. Brunton, et al. 2011. Actomyosin-mediated cellular tension drives increased tissue stiffness and β-catenin activation to induce epidermal hyperplasia and tumor growth. *Cancer Cell*. 19:776–791. http://dx.doi.org/10.1016/j.ccr.2011.05.008

Schlüter, M.A., C.S. Pfarr, J. Pieczynski, E.L. Whiteman, T.W. Hurd, S. Fan, C.J. Liu, and B. Margolis. 2009. Trafficking of Crumbs3 during cytokinesis is crucial for lumen formation. *Mol. Biol. Cell*. 20:4652–4663. http://dx.doi.org/10.1091/mbc.E09-02-0137

Sebbagh, M., M.J. Santoni, B. Hall, J.P. Borg, and M.A. Schwartz. 2009. Regulation of LKB1/STRAD localization and function by E-cadherin. *Curr. Biol.* 19:37–42. http://dx.doi.org/10.1016/j.cub.2008.11.033

Sfakianos, J., A. Togawa, S. Maday, M. Hull, M. Pypaert, L. Cantley, D. Toomre, and I. Mellman. 2007. Par3 functions in the biogenesis of the primary cilium in polarized epithelial cells. *J. Cell Biol.* 179:1133–1140. http://dx.doi.org/10.1083/jcb.200709111

Stinchcombe, J.C., E. Majorovits, G. Bossi, S. Fuller, and G.M. Griffiths. 2006. Centrosome polarization delivers secretory granules to the immunological synapse. *Nature*. 443:462–465. http://dx.doi.org/10.1038/nature05071

Strilić, B., T. Kucera, J. Eglinger, M.R. Hughes, K.M. McNagny, S. Tsukita, E. Dejana, N. Ferrara, and E. Lammert. 2009. The molecular basis of vascular lumen formation in the developing mouse aorta. *Dev. Cell*. 17:505–515. http://dx.doi.org/10.1016/j.devcel.2009.08.011

Théry, M. 2010. Micropatterning as a tool to decipher cell morphogenesis and functions. *J. Cell Sci.* 123:4201–4213. http://dx.doi.org/10.1242/jcs.075150

Théry, M., V. Racine, A. Pépin, M. Piel, Y. Chen, J.B. Sibarita, and M. Bornens. 2005. The extracellular matrix guides the orientation of the cell division axis. *Nat. Cell Biol.* 7:947–953. http://dx.doi.org/10.1038/ncb1307

Vicente-Manzanares, M., M.A. Koach, L. Whitmore, M.L. Lamers, and A.F. Horwitz. 2008. Segregation and activation of myosin IIB creates a rear in migrating cells. *J. Cell Biol.* 183:543–554. http://dx.doi.org/10.1083/jcb.200806030

Wallace, S.W., J. Durgan, D. Jin, and A. Hall. 2010. Cdc42 regulates apical junction formation in human bronchial epithelial cells through PAK4 and Par6B. *Mol. Biol. Cell*. 21:2996–3006. http://dx.doi.org/10.1091/mbc.E10-05-0429

Watanabe, T., H. Hosoya, and S. Yonemura. 2007. Regulation of myosin II dynamics by phosphorylation and dephosphorylation of its light chain in epithelial cells. *Mol. Biol. Cell*. 18:605–616. http://dx.doi.org/10.1091/mbc.E06-07-0590

Wilkinson, S., H.F. Paterson, and C.J. Marshall. 2005. Cdc42-MRCK and Rho-ROCK signalling cooperate in myosin phosphorylation and cell invasion. *Nat. Cell Biol.* 7:255–261. http://dx.doi.org/10.1038/ncb1230

Williams, T., and J.E. Brenman. 2008. LKB1 and AMPK in cell polarity and division. *Trends Cell Biol.* 18:193–198. http://dx.doi.org/10.1016/j.tcb.2008.01.008

Xu, X., T. Omelchenko, and A. Hall. 2010. LKB1 tumor suppressor protein regulates actin filament assembly through Rho and its exchange factor Dbl independently of kinase activity. *BMC Cell Biol.* 11:77. http://dx.doi.org/10.1186/1471-2121-11-77

Yu, W., A. Datta, P. Leroy, L.E. O'Brien, G. Mak, T.S. Jou, K.S. Matlin, K.E. Mostov, and M.M. Zegers. 2005. Beta1-integrin orients epithelial polarity via Rac1 and laminin. *Mol. Biol. Cell*. 16:433–445. http://dx.doi.org/10.1091/mbc.E04-05-0435

Yu, W., A.M. Shewan, P. Brakeman, D.J. Eastburn, A. Datta, D.M. Bryant, Q.W. Fan, W.A. Weiss, M.M. Zegers, and K.E. Mostov. 2008. Involvement of RhoA, ROCK I and myosin II in inverted orientation of epithelial polarity. *EMBO Rep.* 9:923–929. http://dx.doi.org/10.1038/embor.2008.135

Zagórska, A., M. Deak, D.G. Campbell, S. Banerjee, M. Hirano, S. Aizawa, A.R. Prescott, and D.R. Alessi. 2010. New roles for the LKB1-NUAK pathway in controlling myosin phosphatase complexes and cell adhesion. *Sci. Signal.* 3:ra25. http://dx.doi.org/10.1126/scisignal.2000616